| RESEARCH ARTICLE

Finite Element Analysis on Hydroforming of CFRP/SS304 Composite Tube with different Fiber Orientation Stacking Sequence

Felix Thompson Eshun[1] ✉ Talent C.T. Rupango[2] and Wesley Idongesit Umoren[3]

[13]Department of Mechanical and Power Engineering, Nanjing Tech. University, 210009 Nanjing, China
[2]Department of Mechanical Engineering, Nanjing University of Science and Technology, 210094 Nanjing, China
Corresponding Author: Felix Thompson Eshun, **E-mail**: manifesttommy@gmail.com

| **ABSTRACT**

In this paper, a finite element-based approach to the tube hydroforming process of SS304/CFRP material with different stacking sequences was performed in an effort to reveal the failure phases at different stacking angles. The effort to produce hybrid composite tubes through tube hydroforming with composite reinforcement resulted in laminate failure at all the proposed fiber orientation angles. A comparative study of strain energy dissipation at these different stacking angles is further presented. The results show that the $0^0/90^0$ stacking is considered the strongest stacking angle requiring the least strain energy absorption to initial failure of approximately 50 % more as compared to the $\pm30^0$ and $\pm60^0$ stacking angles. The proposed method was more adequate for predicting the strain energy, matrix deformation, and fiber damage when simulating the events.

| **KEYWORDS**

Tube hydroforming, CFRP, Hashin damage, Fiber orientation angle

1. Introduction

Hydroforming is considered one of the potential enabling technologies to deliver lightweight components [Taub et al. 2019]. This cost-effective process of shaping metals into conformed shapes with highly pressurized fluid has become of wide use in industrial sectors to manufacture simple or complex shaped specimen products of use in the automotive and aerospace industrial sectors. In recent years, there has been a considerable increase in the use of hydroforming in the manufacturing industry with faster and more reliable methods. Different methods of implementing hydroforming techniques can be considered based on chosen shape, size, and material being used. To a greater extent, according to the product shape and size, what we need to come up with is based on the geometry used during operation. Composites, either raw or hybrid, have been of much preference recently in aviation, aerospace, chemical, automobile, housing, and other fields mainly due to their high stiffness and strength to weight ratio, flexibility to design, and good resistance to corrosion and fatigue [Bell et al. 2020].

There are many traditional forming processes for carbon fiber composites [Balasubramanian et al. 2018]. However, since carbon fiber reinforced polymers (CFRP) do not possess any yielding or plasticity, they are linear to deformation. With the increased demand for more lightweight and high-strength materials across the industrial manufacturing sector, composites have become more preferable in recent years than conventional metals. Different from the plastic deformation in metal, CFRP generally fails by brittle crushing with multiple micro failure modes, such as matrix cracking, delamination, fiber breakage, etc. [Zhou, 2020]. Much research has been carried out for Steel/CFRP hybrids in terms of crashworthiness, stiffness to certain forces, strength at different temperatures, failure mechanisms, deep drawing structure deformation, and so on [Lee et al. 2017]. As such, this paper aims to perform the tube hydroforming process of Stainless Steel 304 (SS304)/CFRP laminate composite with different fiber orientation stacking sequences which have not yet been employed because of the high stiffness strength ratio of these composites. Karami et

al. [Karami 2015] performed the damage behavior of non-circular metal/composite hybrid vessels subjected to internal pressure with the effect of the fiber orientation on the failure mechanism of the filament wound structures. In his findings, he utilized Hashin's criterion, and the damaged zone extension of shape was greatly influenced by the lay-up configuration of the composite layer and cooperated damage imitation and evolution. A similar approach is implemented in this paper for different fiber orientations and different pressure variations. The main objective of this paper is an initiative to produce lightweight, corrosion-resistant parts of SS304/CRFP, which in automobiles reduces more energy consumption, is environmentally risk-free, and is fairly light in weight.

2. Methodology
2.1. Finite element model
The finite element model of the tube hydroforming process of SS304/CFRP considers five coherent aspects: (1) internal pressure magnitude, (2) axial feed rate, (3) contact relations between surfaces, and (4) the frictional coefficient [Rudraksha, 2020] and (5) the stacking sequence of CFRP composite. The 3D model was developed using the commercial software ABAQUS 2016 to predict the deformation characteristic damage analysis using Hashin with the influence of the applied fluid internal pressure. The model was utilized to reduce computational cost and time, and the geometry of the model has dimensions of 400 mm × 150 mm × 100 mm (length x width x height) for the die mold, as shown in **Fig. 1**.
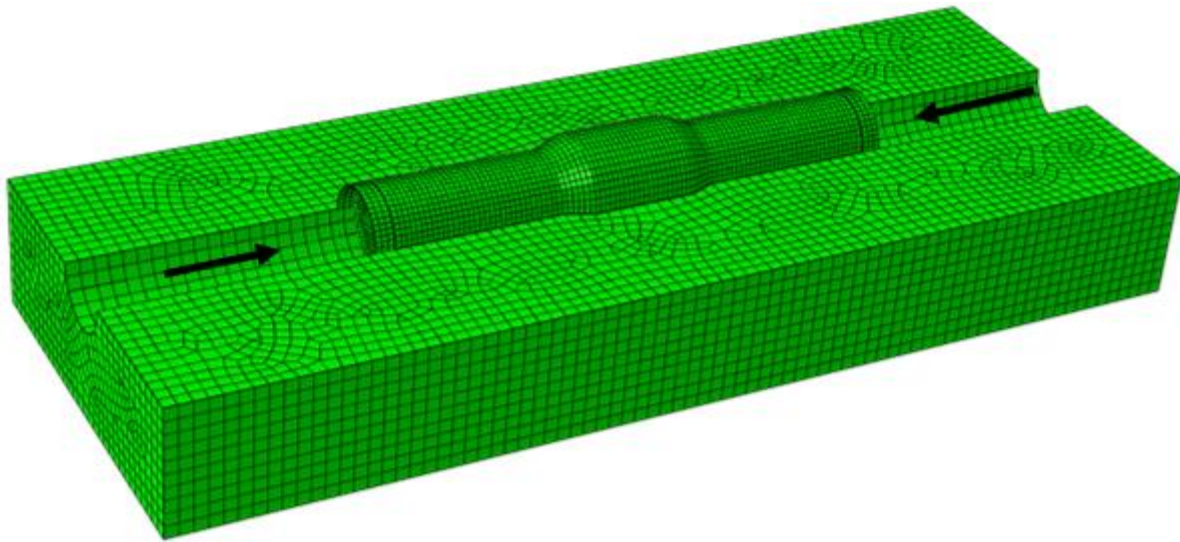

Fig. 1. Mesh Configuration of 3D hydroforming mold, 400 mm × 150 mm × 100 mm (length x width x height).

The ply layup sequence of the CFRP cylindrical tube was considered as $\pm 30^0$, $\pm 60^0$, $0^0/90^0$, which is a two-layer ply stacking with a thickness of 0.5 mm for each ply. The boundary conditions implemented in the finite element model include a fixed encastre on the upper and lower dies to strict any rotational movements in any axis and displacement type to the axial movement on the punches on both ends of the tube. The total thickness T is defined as;

$$T = t_a + t_c \tag{1}$$

were, t_a is the thickness of the SS304 tube and t_c is the thickness of the CFRP, respectively. Both the SS304 and CFRP were meshed using the 4-node doubly curved thin or thick shell, reduced integration (S4R), hourglass control, and finite membrane strains of shell elements, with a total number of elements 4400 and 4700, respectively. The hydroforming mold used was a 3D shell element, and the mesh configuration of the model is shown in **Fig. 1**. The pressure was applied to the inner tube wall, and the pressure profile was modeled to ramp up at a magnitude of 70 MPa, 80 MPa, and 90 MPa.

2.2. Constitutive model
The SS304 tube is considered to be isotropic and elastic-plastic, and the hardening property is adopted to simulate the plastic deformation. The initial length of the tube is considered to be 200 mm, while the inner and outer diameters are 15 mm and 16 mm, respectively. The tested mechanical properties of the SS304 are as follows: the young modulus = 210000 MPa, the yield strength = 215 MPa, and the Poisson ratio = 0.3. It is assumed that the material is isotropic and obeys the hardening rule;

$$\sigma = K\varepsilon^n \tag{2}$$

where σ is the true stress, ε is the true strain and the strength coefficient K was 1425 MPa, and the strain-hardening exponent n value is 0.5

The damage progression algorithm in ABAQUS, known as Hashin's criterion, was employed for modeling of damage initiation and evolution in CFRP composite [Hashin et al. 1980]. A lot of failure criteria have been proposed to predict the damage initiation of composite laminates, thus numerous efforts to improve the damage initiation of laminates. Four failure modes are taken into account: a) fiber tension, b) fiber compression, c) matrix tension, and d) matrix compression. When the corresponding values of fiber and matrix in tension or compression are greater than one means, a damage state has already been initiated. These criteria could be expressed as follows:

Fibre tension ($\sigma_1 \geq 0$) $\quad F_f^t = \left(\frac{\sigma_1}{X^T}\right)^2 + \alpha\left(\frac{\sigma_6}{S^L}\right)^2$ (3)

Fiber compression ($\sigma_1 \leq 0$) $\quad F_f^c = \left(\frac{\sigma_1}{X^C}\right)^2$ (4)

Matrix tension ($\sigma_2 \geq 0$) $\quad F_m^t = \left(\frac{\sigma_2}{Y^T}\right)^2 + \left(\frac{\sigma_6}{S^L}\right)^2$ (5)

Matrix compression ($\sigma_2 \leq 0$) $\quad F_m^c = \left(\frac{\sigma_2}{2S^T}\right)^2 + \left[\left(\frac{Y^C}{2S^T}\right)^2 - 1\right]\frac{\sigma_2}{Y^C} + \left(\frac{\sigma_6}{S^L}\right)^2$ (6)

This failure criterion is used for predicting different failure modes such as fiber breakage in tension, fiber buckling in compression, matrix cracking, and debonding. The elastic constants and the strength properties of CFRP for Hashin's damage initiation criteria are listed in Tables 1 and 2.

Table 1. Elastic and Strength Properties of CFRP [23].

E_1 GPa	E_2 GPa	v_{12}	G_{12} GPa	G_{13} GPa	G_{23} GPa	X^T MPa	X^C MPa	Y^T MPa	Y^C MPa	S^L MPa	S^T MPa
105.5	7.2	0.34	3.4	3.4	2.52	1340	1192	19.6	92.3	51	23

E_1, E_2, and V_{12} are the longitudinal, transversal moduli and Poisson's ratio, respectively; G_{12}, G_{13}, and G_{23} are respective shear moduli; X^T and X^C are the longitudinal tensile and compressive strengths; Y^T and Y^C are transverse tensile and compressive strengths, respectively; and S^L and S^T are shear longitudinal and transverse strengths, respectively.

The constitutive equation of the material when the damage initiation is satisfied, resulting in the degradation of the stiffness of the material, can be expressed as a relation between stress and strain as:

$$\begin{bmatrix}\sigma_1 \\ \sigma_2 \\ \sigma_6\end{bmatrix} = \frac{1}{D}\begin{bmatrix}(1-d_f)E_1 & (1-d_f)(1-d_m)v_{12}E_1 & 0 \\ (1-d_f)(1-d_m)v_{12}E_2 & (1-d_m)E_2 & 0 \\ 0 & 0 & (1-d_s)GD\end{bmatrix}\begin{bmatrix}\varepsilon_1 \\ \varepsilon_2 \\ \varepsilon_6\end{bmatrix}$$ (7)

Where d_f, d_m, and d_s are damage variables within 0 and 1, representing the fiber breakage, matrix cracking, and shear failure, respectively, with D $=1-(1-d_f)(1-d_m)v_{12}v_{21}$ and $d_s = 1-(1-d_f^t)(1-d_f^c)(1-d_m^t)(1-d_m^c)$, E_1, E_2, and G_{12} are material moduli of undamaged status, and $v_{12 \text{ and }}v_{21}$ are undamaged material Poisson's ratios in the local coordinate system of the material.

Table 2. Damage Properties of CFRP

Longitudinal tensile fracture energy, N/mm	Longitudinal compressive fracture energy, N/mm	Transverse tensile fracture energy	Transverse compressive fracture energy, N/mm
48.4	60.3	4.5	8.5

3. Results and Discussions

3.1 *Thickness distributions across the tube sections*

Separate pre-simulations proved that for the proposed pressure values, the SS304 metal does not exhibit any wrinkling, buckling, or bursting, which are the main issues in tube hydroforming [Tang et al. 2020], and the thickness distributions across the tube sections are shown below in **Fig. 2**. From Fig. 2, the expansion zone (A) is where the parts take the geometric shape on the cavity, the transition zone (B) is when internal pressure and axial compressional force act on the workpiece, and the guided zone (C) has little expansion of the surface or basically no deformation. The thickness variation decreases steadily from time t = 0 to t = 0.0043 and becomes constant until the simulation is completed. The thickness variation is higher across section B as compared to A and C.
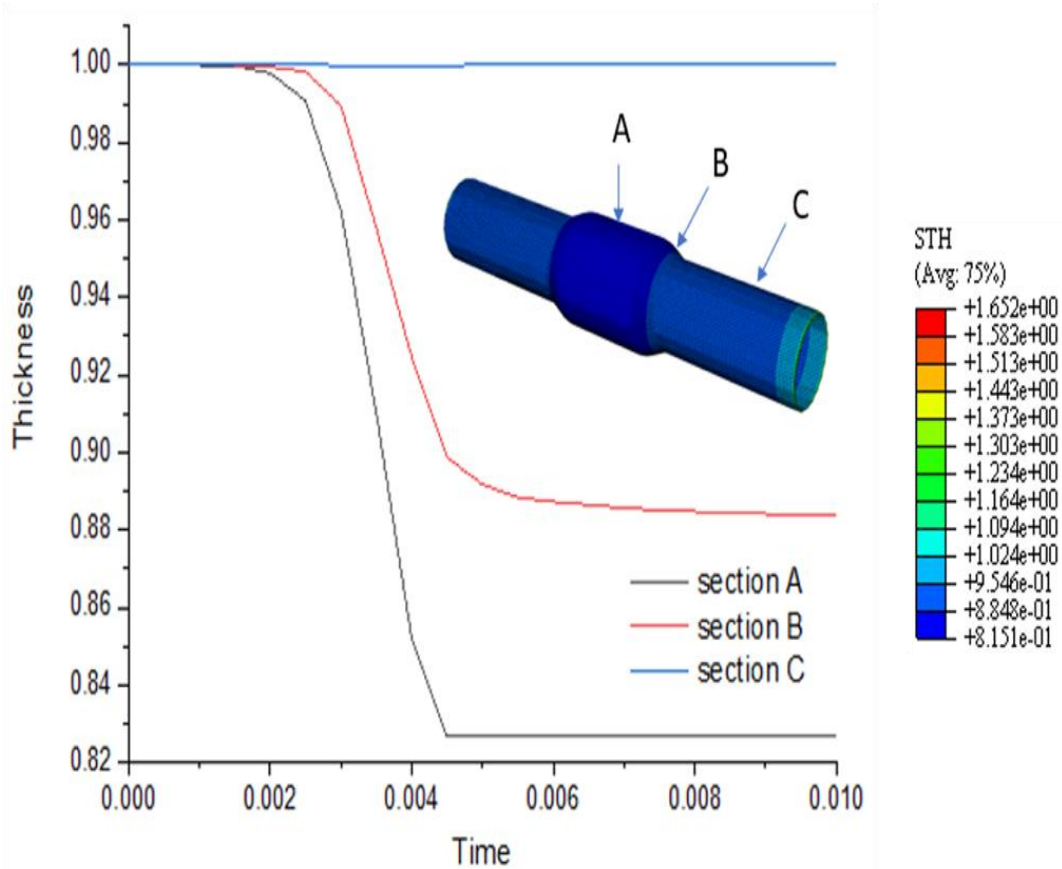

Fig. 2. Thickness variations across the tube sections at 90 MPa

3.2 *Effect of stacking angle*

The stacking angle for each layup exhibits different CFRP failure phases. Fiber angle orientation and stacking sequence have robust effects on the toughness of CFRPs on laminate fracture [Naghipour, 2010]. The $0^0/90^0$ stacking is considered the stronger stacking angle requiring at least strain energy absorption to initial failure, approximately 50% more as compared to the $\pm30^0$ and $\pm60^0$ stacking angles (**Fig. 3**). Laminate failure is also achieved in phases $\pm30^0$ (Fig. 3A), $\pm60^0$ (Fig. 3B) stacking angles with the first ply failure before the preceding ply fails also. A drop in stored strain energy is an indication of the first failure to the sufficient pressure acting on the adjutant face of the ply in terms of the stacking angles offering more stiffness to deformation as compared to $0^0/90^0$ stacking angles (Fig. 3C). As such the evolution of the strain energy on the $0^0/90^0$ stacking angle as the damage propagates was further examined as shown in Fig. 3C. It can be observed that the critical energy is higher for 70 MPa strain energy, showing that after absorbing a specific amount of strain energy, the laminate material loses its load-bearing capacity while the strain energy abruptly falls and then the fiber matrix fails. The other pressure variations have a slight percentage difference with approximate critical energy of at least 16% lower than the first.
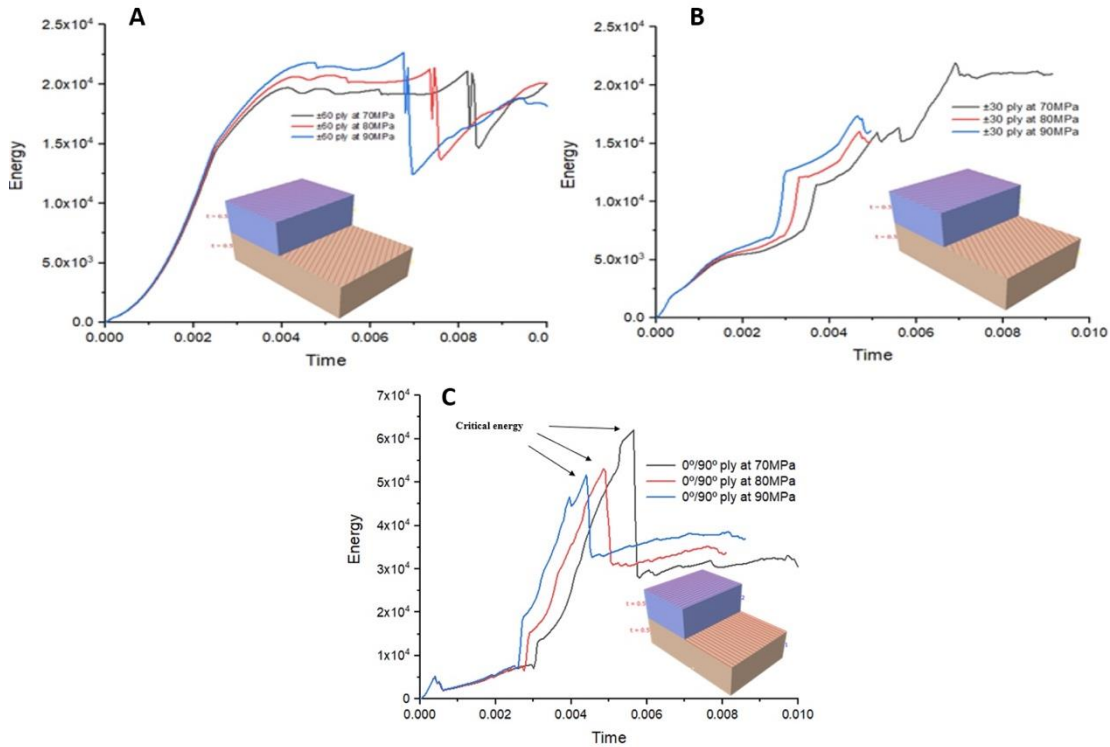
Fig 3. Evolution of the strain energy the (A) ±30^0 (B) ±60^0 and (C) 0^0/90^0 stacking angle as the damage propagates.

3.3 Model Damage Analysis

The fiber orientation has a significant effect on laminate failure. **Fig. 4**(a)-(c) shows the proposed fiber orientation angles. The fibers oriented between 0°/90° (Fig. 4(a)) better reinforce the composite structure and mitigate the crack propagation regardless of its orientation, thus giving more stiffness and toughness than other proposed fiber orientation angles. The effort to produce hybrid composite tubes through tube hydroforming with composite reinforcement resulted in laminate failure at all the proposed fiber orientation angles, particularly at ±60^0. The strong correlation observed proves that CFRPs are brittle, crack then break rather than SS, which are ductile and undergo elastic deforming, showing bending first before failure or breaking.
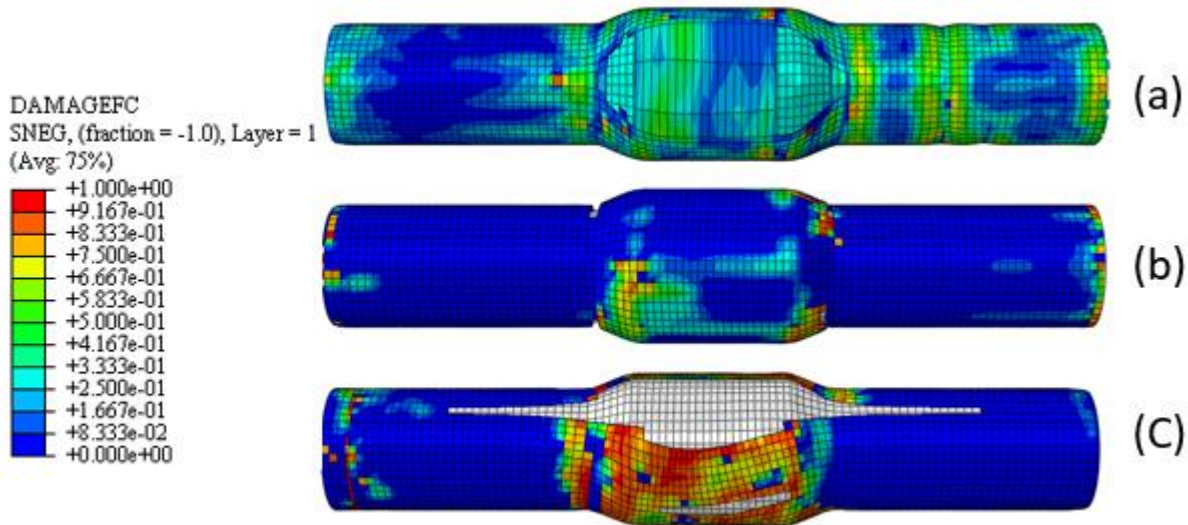

Fig. 4. Fiber compression damage pattern for different lay-up configurations (a) 0°/90° (b) ±30^0 (c) ±60^0

Next, we model the fiber damage for ply 0°/90° stacking since the fibers oriented between 0°/90° (Fig. 4(a)) produced a better reinforced composite structure. From **Fig. 5**, the fiber failure resulted in the CFRP tearing up in all pressure instances since the

value around the bulge is greater than one. The inner metal, however, is affected at the point along the die as the fiber fails but does not result in failure of the metal or piercing in some manner. The ends experience similar failure deformations in the early stages of the deformation process.
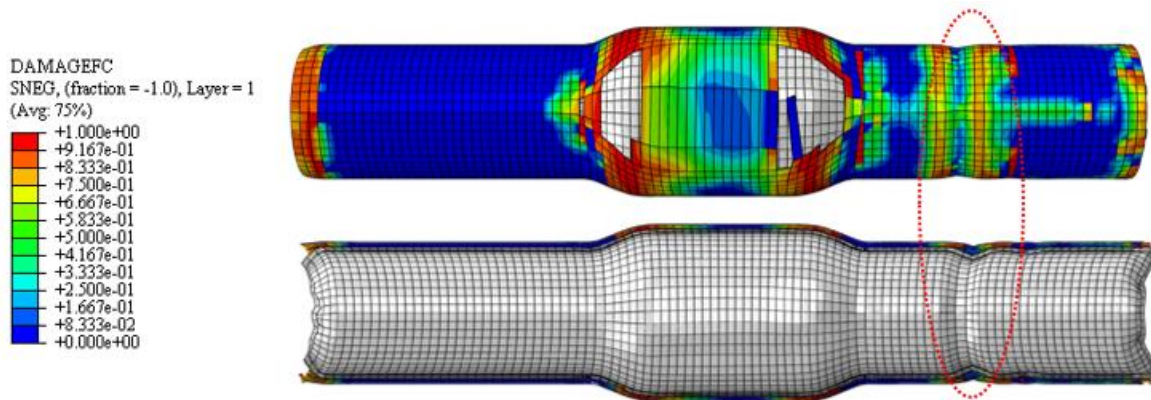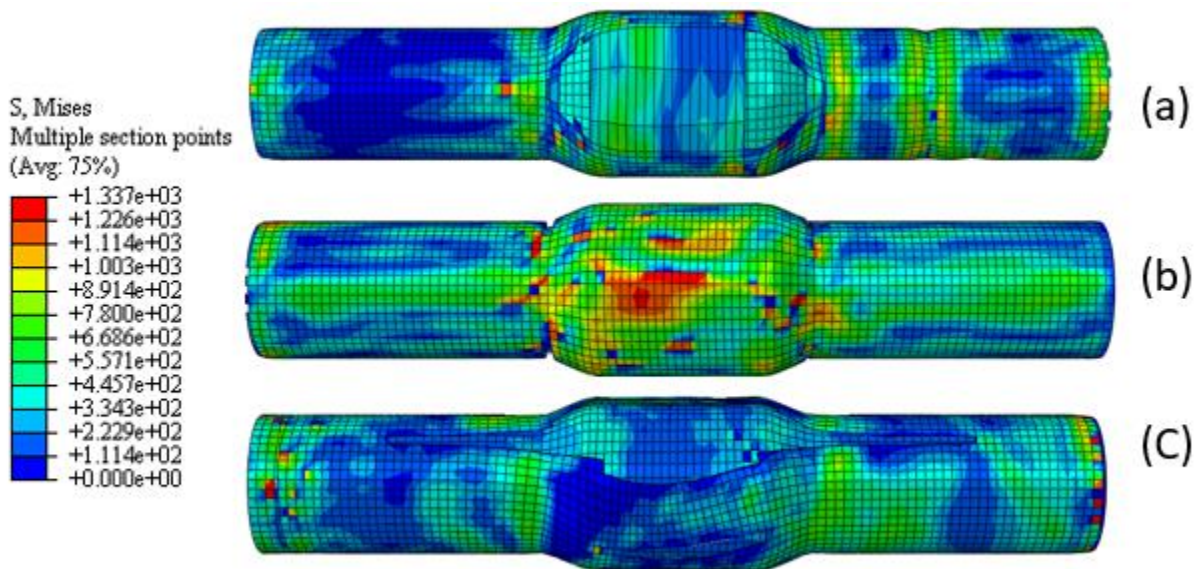

Fig 5. Fiber damage for ply 0°/90° stacking

Fig 6. Von Mises stress field configurations (a) 0°/90° (b) $\pm30^0$ (c) $\pm60^0$ at 90 MPa

Fig. 6 shows the evolution of Mises stress for the tube after the simulation with the maximum value of 90 Mpa at different configurations. The endpoints of the configurations experienced the most stress, while $\pm30^0$ buckled more at the bulges. The ends of the tube tend to buckle in, and these are cut out and refined later after the process is finished. Thickness variations can spread throughout the structure of the tube with greater dissipation around the bulge areas.

4. Conclusions
In this paper, the hydroforming of SS304/CFRP laminate composite with different fiber orientation stacking sequences was examined through finite element simulation using ABAQUS 2016. The $0^0/90^0$ stacking is considered the strongest stacking angle requiring the least strain energy absorption to initial failure of approximately 50 % more as compared to the $\pm30^\circ$ and $\pm60^\circ$ stacking angles. The Mises stress for the tube after the simulation with the maximum value of 90 MPa at different configurations shows that the endpoints of the configurations experienced the most stress, while $\pm30^0$ buckled more at the bulges. The effort to produce hybrid composite tubes through tube hydroforming with composite reinforcement resulted in laminate failure at all the proposed fiber orientation angles. Finally, the strong correlation observed proves that CFRPs are brittle, crack then break rather than SS, which are ductile and undergo elastic deforming, showing bending first before failure or breaking.

Conflicts of Interest: The authors declare no conflict of interest
Publisher's Note: All claims expressed in this article are solely those of the authors and do not necessarily represent those of their affiliated organizations, or those of the publisher, the editors and the reviewers.

Reference

[1] Balasubramanian, K., M.T. Sultan, & N. Rajeswari, (2018). Manufacturing techniques of composites for aerospace applications, in Sustainable Composites for Aerospace Applications. *Woodhead Publishing, Elsevier*. 55-67.

[2] Bell, C., Corney, J. & Zuelli, N., (2020). A state-of-the-art review of hydroforming technology. *International Journal of Material Forming, 13*(5) 789-828.

[3] Chandrathilaka, E.R.K., Gamage, J.C.P.H. & Fawzia, S., (2019). Mechanical characterization of CFRP/steel bond cured and tested at elevated temperature. *Composite Structures, 207,* 471-477.

[4] Han, S., Woo, Y., Hwang, T., Oh, I. & Moon, Y.H., (2019). Tailor layered tube hydroforming for fabricating tubular parts with dissimilar thicknesses. *International Journal of Machine Tools and Manufacture, 138,* 51-65.

[5] Heggemann, T., & Homberg, W. (2019). Deep drawing of fiber metal laminates for automotive lightweight structures. *Composite Structures*, 216, 53-57.

[6] Hashin, Z. (1980). Failure criteria for unidirectional fiber composites.

[7] Hashin, Z., & Rotem, A. (1973). A fatigue failure criterion for fiber reinforced materials. *Journal of composite materials, 7*(4), 448-464.

[8] Jamir, M.R., Majid, M.S. & Khasri, A., (2018). Natural lightweight hybrid composites for aircraft structural applications. In Sustainable composites for aerospace applications, Woodhead Publishing, Elsevier. 155-170.

[9] Karami, P., Tabatabaei, S. A., Zangaraki, R., & Mashhadi, M. M. (2015). Experimental and numerical analyses of progressive damage in non-circular metal/composite hybrid vessels under internal pressure. *International Journal of Damage Mechanics, 24*(8), 1261-1279.

[10] Kong, T. F., Lu, X. Z., & Chan, L. C. (2019). Analysis and reduction of wrinkling defects for tube-hydroforming magnesium alloy components at elevated temperatures. *Materials & Design, 173,* 107761.

[11] Lee, M.S., Seo, H.Y. & Kang, C.G., (2017). Comparison of collision test results for center-pillar reinforcements with TWB and CR420/CFRP hybrid composite materials using experimental and theoretical methods. *Composite Structures, 168*, 698-709.

[12] Naghipour, P., Bartsch, M., Chernova, L., Hausmann, J., & Voggenreiter, H. (2010). Effect of fiber angle orientation and stacking sequence on mixed mode fracture toughness of carbon fiber reinforced plastics: Numerical and experimental investigations. *Materials Science and Engineering: A, 527*(3), 509-517

[13] Rajak, D.K., Pagar, D.D., Kumar, R. & Pruncu, C.I., (2019). Recent progress of reinforcement materials: a comprehensive overview of composite materials. *Journal of Materials Research and Technology, 8(*6) 6354-6374.

[14] Rudraksha, S. P., & Gawande, S. H. (2020). Influence of lubricants on the coefficient of friction in tube hydroforming. *Journal of Bio-and Tribo-Corrosion, 6*(1), 1-8.

[15] Rahimian Koloor, S. S., Karimzadeh, A., Yidris, N., Petrů, M., Ayatollahi, M. R., & Tamin, M. N. (2020). An energy-based concept for yielding multidirectional FRP composite structures using a mesoscale lamina damage model. *Polymers, 12*(1), 157.

[16] Rajak, D.K., Pagar, D.D., Menezes, P.L. & Linul, E., (2019). Fiber-reinforced polymer composites: Manufacturing, properties, and applications. *Polymers, 11*(10) 1667.

[17] Ra, J. H., Han, S. W., VanTyne, C. J., & Moon, Y. H. (2019). Manufacturing of a wire-reinforced aluminum tube via hydroforming process. *International Journal of Machine Tools and Manufacture, 143*, 1-15.

[18] Sun, G., Wang, Z., Hong, J., Song, K. & Li, Q., (2018). Experimental investigation of the quasi-static axial crushing behavior of filament-wound CFRP and aluminum/CFRP hybrid tubes. *Composite Structures, 194*, 208-225.

[19] Swift, K. & Booker, J.D., (2013). Chapter 5-Plastics and Composites Processing. Manufacturing Process Selection Handbook. 141-174.

[20] Schäfer, J. & Gries, T., (2016). Braiding pultrusion of thermoplastic composites. In Advances in Braiding Technology. *Woodhead Publishing, Elsevier*. 405-428.

[21] Sung, M., Jang, J., Hong, S. T., & Yu, W. R. (2020). Increased breaking strain of carbon fiber-reinforced plastic and steel hybrid laminate composites. *Composite Structures, 235*, 111768.

[22] Tang, Z. J., Gang, L. I. U., He, Z. B., & Yuan, S. J. (2010). Wrinkling behavior of magnesium alloy tube in warm hydroforming. Transactions of Nonferrous Metals Society of China, 20(7), 1288-1293.

[23] Taub, A., De Moor, E., Luo, A., Matlock, D.K., Speer, J.G. & Vaidya, U., (2019). Materials for automotive lightweighting. *Annual Review of Materials Research, 49*(1) 327-359.

[24] Uriayer, F. A., & Alam, M. (2013). Mechanical properties of steel-CFRP composite specimen under uniaxial tension. Steel Compos. *Struct., Int. J, 15*(6), 659-677.

[25] Wollmann, T., Hahn, M., Wiedemann, S., Zeiser, A., Jaschinski, J., Modler, N., Khalifa, N.B., Meißen, F. & Paul, C., (2018). Thermoplastic fibre metal laminates: Stiffness properties and forming behaviour by means of deep drawing. *Archives of Civil and Mechanical Engineering, 18(*2), 442-450.

[26] Yuan, S., Yuan, W., & Wang, X. (2006). Effect of wrinkling behavior on formability and thickness distribution in tube hydroforming. Journal of materials processing technology, 177(1-3), 668-671.

[27] Zhou, G., Sun, Q., Fenner, J., Li, D., Zeng, D., Su, X. & Peng, Y., (2020). Crushing behaviors of unidirectional carbon fiber reinforced plastic composites under dynamic bending and axial crushing loading. *International Journal of Impact Engineering,* 140, 103539.